IEEE Access
Multidisciplinary | Rapid Review | Open Access Journal

Received November 19, 2018, accepted December 13, 2018, date of publication December 21, 2018,
date of current version January 11, 2019.

Digital Object Identifier 10.1109/ACCESS.2018.2889219

OFDM Modulated PNC in V2X Communications: An ICI-Aware Approach Against CFOs and Time-Frequency-Selective Channels

ZHENHUI SITU[1], IVAN WANG-HEI HO[1,2], (Senior Member, IEEE), TAOTAO WANG[3,4], (Member, IEEE), SOUNG CHANG LIEW[4], (Fellow, IEEE), AND SID CHI-KIN CHAU[5], (Member, IEEE)

[1]Department of Electronic and Information Engineering, The Hong Kong Polytechnic University, Hong Kong
[2]Research Institute for Sustainable Urban Development, The Hong Kong Polytechnic University, Hong Kong
[3]College of Information Engineering, Shenzhen University, Shenzhen 518060, China
[4]Department of Information Engineering, The Chinese University of Hong Kong, Hong Kong
[5]Research School of Computer Science, The Australian National University, Canberra, ACT 0200, Australia

Corresponding author: Ivan Wang-Hei Ho (ivanwh.ho@polyu.edu.hk)

The work of I. W.-H Ho was supported in part by the General Research Fund established under the University Grant Committee (UGC) of the Hong Kong Special Administrative Region (HKSAR), China, under Project 15201118, and in part by The Hong Kong Polytechnic University under Project G-YBK6 and Project G-YBR2. The work of Z. Situ was supported in part by the National Natural Science Foundation of China under Project 61401384. The work of T. Wang and S. C. Liew was supported in part by the Innovation and Technology Fund established under the Innovation and Technology Commission of the Hong Kong Special Administrative Region, China, under Project ITF/447/16FP.

ABSTRACT This paper studies the application of physical-layer network coding (PNC) in vehicle-to-everything communications to accommodate the time-critical nature of vehicular ad-hoc networks (VANETs). The idea can theoretically reduce the transmission latency by 50%, thus alleviating the short contact time issues caused by high-speed vehicle motion. Conventional studies of PNC primarily considered static networks. In highly mobile networks like VANETs, the carrier frequency offsets (CFOs) due to high-speed motion will lead to inter-carrier interference (ICI) in orthogonal frequency division multiplexing (OFDM) systems. Moreover, the vehicular environment with time–frequency-selective channels further undermines accurate channel estimation for multiple users. It is also worth noting that the CFO that exists in OFDM modulated PNC cannot be completely eliminated through CFO tracking and equalization as in conventional point-to-point transmissions. These critical issues can significantly increase the bit error rate at the receiver. To address these challenges, this paper proposes an ICI-aware approach that jointly achieves accurate channel estimation, signal detection, and channel decoding. We express the channel estimation and detection and decoding as two optimization problems and resolve them with the expectation–maximization algorithm and the belief propagation algorithm, respectively. The proposed approach can efficiently mitigate the negative effect of ICI by exploiting both pilot and data tones in channel estimation, detection, and decoding. Both simulation and experiment are conducted to evaluate the proposed approach, and the results reveal that the proposed algorithm outperforms the benchmark that simply treats ICI as Gaussian noise.

INDEX TERMS V2X communication, physical-layer network coding, time-frequency-selective channel, inter-carrier interference.

I. INTRODUCTION

Vehicle-to-everything (V2X) communications, which incorporates vehicular communications such as Vehicle-to-Infrastructure (V2I), Vehicle-to-Vehicle (V2V), Vehicle-to-Pedestrian (V2P) and so on, are attracting increasing attention in both academia and industry. By enabling information exchange among vehicles and everything with wireless communication components, V2X communications improve traffic safety and offer various services. For example, to enable the 5th level of automation [1], communications among vehicles as well as the road infrastructure is a must for overcoming the challenges in every driving scenario including

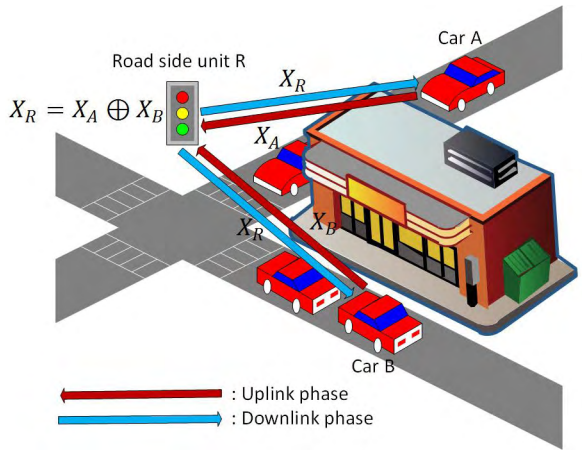

FIGURE 1. A TWRC that operates with OFDM modulated PNC.

extreme environments. Dedicated short-range communications (DSRC) is used in the US for V2X communications. This protocol stack applies 802.11p to the PHY and MAC layers, and the 5.85-5.925 GHz band is allocated for DSRC. Recently, Cellular V2X (C-V2X) was proposed in 3GPP release 14 [2], it is employed in the 5G Automotive Association (5GAA) for safety and cooperative driving.

Although broadcast is commonly used in Vehicular Ad-hoc Networks (VANETs) for safety beacons and emergency warning, two way relay transmission can be used at a road junction for exchanging data between vehicles on different road segments. In Fig. 1, two semi-automated cars A and B record the traffic information within their detection range, and want to share the information with each other. However, the radio channel between them is obstructed by buildings. The two cars thus need a road-side unit R to forward the data for them. In conventional communication systems, car A sends package X_A to the relay, then the relay forwards X_A to B. Similarly, car B spends two time slots to send packages X_B to car A. It takes totally four time slots to finish the package exchange in such a two-way relay channel (TWRC), which is time consuming and not suitable for the time-critical nature of VANETs.

A technique to reduce the latency in Fig, 1 by harnessing wireless interference is physical-layer network coding (PNC) [3]. Specifically, PNC divides the data exchange into two phases: the uplink phase and downlink phase. In the uplink phase, two cars A and B simultaneously transmit signals X_A and X_B to relay R. Undergoing channels A and B respectively, signals X_A and X_B overlap at relay R. Then, R detects and decodes the overlapped signal to obtain the exclusive or (XOR) output of the two transmitted signals, $X_R = X_A \oplus X_B$. After that, relay R broadcasts X_R in the downlink phase. Finally, the two cars A and B recover their desired data with self information (e.g., car A can recover the data from car B via $X_B = X_A \oplus X_R$). The number of time slots required for the same data exchange is reduced from four to two, which indicates a 50% latency reduction.

Both V2X communications and PNC are not new research topics. However, to the best of our knowledge, there are not many investigations on applying PNC to vehicular communications. Notice that most previous studies on PNC assume that the nodes are static since mobile node will create a lot of issues on channel estimation, signal synchronization, etc. This paper studies a TWRC operated Orthogonal frequency division multiplexing (OFDM) modulated PNC.

Different from the conventional point-to-point (P2P) communications, CFO originated from imperfect local oscillators at the two end nodes and Doppler spreads is inevitable in PNC systems (two CFOs from the two end nodes are probably different and thus they cannot be completely eliminated). It varies the relative channel gain, which includes phase offset and power difference between the two end nodes and causes inter-carrier interference (ICI) among OFDM subcarriers [4]. Pan *et al.* [5] revealed that the uncontrollable phase offset creates the XOR mapping ambiguity regardless of the noise. The minimum Euclidean distance between two points that belong to different XOR mappings does not only depend on the signal strength but also the relative channel gain [6]. In this case, the ICI can lead to severe performance degradation. Operating in vehicular network, these issues are further enlarged by the time-frequency-selective channels owing to the multi-path and high-mobility environment [7]. Most previous channel estimation algorithms for PNC such as linear interpolation [8] are designed based on the assumption of static network. They are simple and provide reasonable performance under static network, but cannot track the rapidly changing channel conditions in V2X communications [7].

Basis expansion model (BEM) [9] is a powerful tool to capture the time-varying channel with a few modeling coefficients. The model facilitates channel estimation by significantly reducing the number of unknown parameters to be estimated. In addition, BEM-based estimator can track channel responses for not only desired signals but also ICI, thus providing the solution to tackle the negative effect of ICI. However, the previous BEM-based schemes use only orthogonal pilots to achieve channel estimation. For PNC systems, multi-user access decreases the number of pilot tones for each user, thus degrading the estimation accuracy. Attentive to this limitation, this paper exploits not only orthogonal pilot but also non-orthogonal data tones to achieve BEM-based channel estimation and decoding for PNC systems.

The objective of this work is to achieve accurate channel estimations and mitigate the ICI caused by CFO in signal detection and channel decoding in highly-mobile PNC channel. We propose an iterative scheme that can efficiently address the negative effects induced by time-frequency-selective channels and ICI in V2X communications. The salient features of the proposed algorithm are three-fold:

1) As far as we know, there is no previous investigation on time-frequency-selective channel estimation for PNC. However, double-selective channels must be considered in vehicular environments due to the multi-path nature and the Doppler effect. Based on the

expectation maximization (EM) algorithm, we firstly apply the BEM to convert the channel estimation task to solving a linear problem. Besides, the estimation is optimized by taking ICI and all tones into consideration.

2) Suffering from the detrimental effects of CFO and double-selective channels, the distance between two XOR mappings in the constellation can be very short. In this case, not only noise but also ICI will significantly affect the signal detection and channel decoding. We exploit the belief propagation (BP) algorithm [10] and an ICI-aware method to mitigate ICI in the detection and decoding phase.
3) Both the EM and BP algorithms can be enhanced with more number of iterations, the proposed method iterates between 1) and 2) to improve channel estimation, detection and decoding progressively. The simulation results show that the proposed approach can converge within three iterations.

The remainder of this paper is organized as follows. Section II reviews related work. We describe the system model of this work in Section III. Section IV discusses the proposed method in terms of two parts: the channel estimation part and the detection and decoding part. Then, Section V analyzes the computational complexity of the proposed algorithm. After that, simulation results are presented and analyzed in Section VI. Besides, we provide the experimental results in VII to further verify the proposed scheme. Finally, Section VIII concludes the paper.

II. RELATED WORK

PNC was first proposed in [3] and [11]. For the application of PNC in V2X communications, Ndih and Cherkaoui [12] focused on the MAC layer and proposed a MAC protocol. The feasibility of PNC in V2X communications was first studied in [13]. The major interest was the effect of CFO and it was found that in the worst case, PNC in V2X communications suffers only at most a 3 dB SINR penalty compared with conventional P2P communications. This work considers ICI-aware channel estimation and decoding for PNC in V2X communications, which were not covered in [13].

In terms of channel estimation in PNC, Wang and Liew [14] customized a joint channel estimation and channel decoding framework for PNC. But this work only considered single-carrier systems without CFO. In addition, the framework is also not applicable to OFDM based PNC with CFO. For OFDM-based PNC, Lu *et al.* [8] adopted time-orthogonal (time non-overlapping) training symbols and pilots for the two end nodes. In this case, the channel estimation problem in PNC is reduced to that of traditional communication systems since the two channels are estimated separately. A low-overhead channel precoding system was proposed for mobile lattice-coded PNC in [15]. The algorithm requires feedback to align the channels. However, the approach only considered single-path channel estimation and the ordinary walking speed in the conducted experiment was insufficient for V2X communications. These above works did not consider channel estimation under time-frequency-selective channels. To cope with the double-selective channel estimation, various algorithms had been proposed [16]–[18], but these algorithms are designed for P2P communications. It is uncertain that whether they are feasible to estimate the overlapped signal or not.

A common method to mitigate ICI induced by CFO is interference cancellation. Before channel estimation and decoding, ICI is removed with the use of ICI coefficients and decoded data [4], [19], [20]. Therefore, the channel estimation and decoding are assumed to be conducted under interference-free situation. The cancellation can be further divided into hard and soft cancellations depending on whether the data information is obtained from a hard (binary value) decision or a soft (mean value) decision. In [21], the effect of CFO was discussed in depth and ICI was considered in form of the a posteriori probability (APP). However, these works focused on CFO but assumed channel to be known (i.e., the issue of channel estimation was not addressed). Finally, Wang *et al.* [22] tracked the phase offset on the target subcarrier caused by CFO under flat fading channel and frequency selective channel. However, it neglected the effect of ICI.

Compared with previous works, this paper takes both channel estimation under time-frequency-selective channels, and detection and decoding under ICI into account. These two critical issues are addressed for PNC in vehicular environments.

III. SYSTEM MODEL

This paper studies the TWRC illustrated in Fig. 1. Since the downlink phase can be considered as traditional broadcasting, this work focuses on the most challenging part: the uplink phase. We first depict the mobile radio channels adopted for the two end nodes. Then the overlapping signal at the relay is discussed and we can see the negative effect of double-selective channels and CFOs. The third and forth subsections study the impact of relative channel gain and ICI on PNC systems. Finally, the last subsection shows how the BEM transfers the complicated superimposed signals into a simple linear equation.

A. TIME-FREQUENCY-SELECTIVE CHANNELS

In V2X communications, the multi-path environment and high mobility of vehicles create a lot of complexity in the mobile radio channels. The transmitted signals are propagated through multiple paths and mingle at the receiver. And the signals from different paths experience different delay and path gain. The signals suffer from delay spread and the maximum delay can be up to hundreds of ns [23]. Under high speed, signals with different incident angles have diverse Doppler shifts, and the maximum Doppler frequency in V2X communications is around 1500 Hz [24]. Previous empirical channel models [23], [24] indicate that the consideration of double-selective channels in V2X communications

is necessary. In this work, we assume that the signals from the two end nodes undergo two independent time-frequency-selective channels characterized by wide-sense stationary uncorrelated scattering (WSSUS) models [25]. Specifically, the time-variant impulse response can be described as

$$h_i(\tau_i, t) = \sum_{p_i=1}^{P_i} c_{p_i}(t)\delta(\tau_i - \tau_{p_i}) \tag{1}$$

where $i \in \{A, B\}$ is the label for the two end nodes, P_i indicates the total number of propagation paths with different delays. t means the time, $\delta(\tau_i - \tau_{p_i}) = 0$ when $\tau_i \neq \tau_{p_i}$ and $\delta(\tau_i - \tau_{p_i}) = 1$ when $\tau_i = \tau_{p_i}$. For the p_i-th path with delay τ_{p_i}, we consider non-line-of-sight (NLOS) propagation and the complex channel gain $c_{p_i}(t)$ is modeled as a Rayleigh process that follows the Jakes' power spectrum [25] with maximum Doppler frequency f_{d_i}:

$$f_{d_i} = \frac{v_i}{c} f_c \tag{2}$$

where c indicates the speed of electromagnetic waves, v_i is the relative velocity between the transmitter and receiver (e.g., high speed that is up to 100 km/hr), and f_c is the carrier frequency. In addition to the Doppler spread, we assume that the imperfection of the local oscillators used to generate the radio frequency (RF) at the two end nodes A and B causes frequency offset f_{δ_i}. The imperfect local oscillators and the rapid motion of vehicles make CFO inevitable in V2X communications.

B. SUPERIMPOSED OFDM SIGNALS

According to the 802.11p standard, we consider OFDM modulated PNC for V2X communications. The source data S_A and S_B, which are binary data, is first channel encoded, interleaved, and mapped to the constellation via modulation (e.g., BPSK and QPSK). After that we obtain channel encoded and modulated data X_A and X_B. The inverse fast Fourier transform (IFFT) will then change the modulated data from frequency domain to time domain. After adding the cyclic prefix (CP), the time-domain signals are ready to be transmitted. Here the number of subcarriers is M and the length of CP is G. An important assumption in this work is that we assume CP can successfully cover the maximum delay so that the inter-symbol interference (ISI) can be eliminated. This is practicable by setting the length of CP sufficient. Let the bandwidth be B and the sampling rate is configured to be $B = 1/T_s$, where T_s indicates the sampling interval. The duration of one symbol is $T = (M + G)T_s$. One data frame contains L symbols. The transmitted time-domain baseband discrete signals from node i at the l-th symbol is represented as

$$x_i[q + G + (l-1)(M+G)] = \frac{1}{M} \sum_{m=-M/2}^{M/2-1} X_{i,l}[m] e^{j2\pi \frac{m}{M} q} \tag{3}$$

where q is the time index within a symbols, and $X_{i,l}[m]$ is the modulated information mapped from binary bit to the constellation. After up conversion, propagating through the mobile radio channels described in (1), and down conversion, the baseband signals from the two end nodes A and B overlap at the relay R, and we can express it as follows

$$y(t) = \sum_{i \in \{A,B\}} (x_i(t) \otimes h_i(\tau_i, t)) e^{j2\pi f_{\delta_i} t} + n(t) \tag{4}$$

where $\otimes$ denotes convolution operation, $n(t)$ is the complex white Gaussian noise with zero mean and variance σ_t^2. In the following, we further consider the product of $h_i(\tau_i, t)$ and the CFO due to oscillator imperfection $e^{j2\pi f_{\delta_i} t}$ to be one single component $h_i(\tau_i, t)$. This is reasonable since the hardware frequency offset can be regarded as part of the Doppler spread without loss of generality and this helps to simplify the equation. By performing fast Fourier transform (FFT) operation, the frequency-domain signal on the l-th symbol is given by

$$\boldsymbol{Y}_l = \boldsymbol{H}_{A,l}\boldsymbol{X}_{A,l} + \boldsymbol{H}_{B,l}\boldsymbol{X}_{B,l} + \boldsymbol{W}_l. \tag{5}$$

Here we use bold capital letters to denote arrays (e.g., vector or matrix). The above equation contains three $M \times 1$ vectors, which are $\boldsymbol{Y}_l$, $\boldsymbol{X}_{i,l}$ and $\boldsymbol{W}_l$, and two $M \times M$ matrices, which are $\boldsymbol{H}_{A,l}$ and $\boldsymbol{H}_{B,l}$. $\boldsymbol{Y}_l$ and $\boldsymbol{X}_{i,l}$ include data information of M subcarriers. $\boldsymbol{W}_l$ contains the independent noise on each subcarrier, and the noise is zero mean with variance $\sigma_f^2 = M\sigma_t^2$. $\boldsymbol{H}_{i,l}$ contains the detailed channel gains for one symbol. The diagonal elements $\boldsymbol{H}_{i,l}[m, m]$ denote complex channel responses for desired signals on the target subcarriers, while other elements are coefficients for ICI. (the non-diagonal elements should be zero when there is no CFO). The frequency-domain impulse response from subcarrier k to subcarrier m can be interpreted as follows:

$$\boldsymbol{H}_{i,l}[m, k] = \sum_{p_i=1}^{P_i} \alpha_t(m, k, l, p_i)\alpha_f(k, p_i), \tag{6}$$

with

$$\begin{aligned} \alpha_t(m, k, l, p_i) &= \frac{1}{M} \sum_{q=0}^{M-1} c_{p_i}((q+G)T_s + (l-1)T) \\ &\quad \times e^{j2\pi \frac{k-m}{M} q}, \\ \alpha_f(k, p_i) &= e^{-j2\pi k \Delta f \tau_{p_i}}. \end{aligned} \tag{7}$$

The impulse response is the summation of impulse responses from all paths. For each path, the impulse response is the product of $\alpha_t(m, k, l, p_i)$ and $\alpha_f(k, p_i)$. $\alpha_t(m, k, l, p_i)$ is the output coefficient of the signal on the k-th subcarrier to the m-th subcarrier at the l-th symbol. It reflects the time-varying characteristic. $\alpha_f(k, p_i)$ is a phase rotation caused by delay τ_{p_i}. It shows the frequency-varying characteristic. $\Delta f = 1/(MT_s)$ is the subcarrier spacing. If only one path exists, the channel is frequency-flat, which means the amplitudes of impulse responses on all subcarriers are the same. Multi-path leads to frequency-selective channels. $\boldsymbol{H}_{i,l}[m, k]$ with $m \neq k$ indicates ICI coefficient. Previous work on

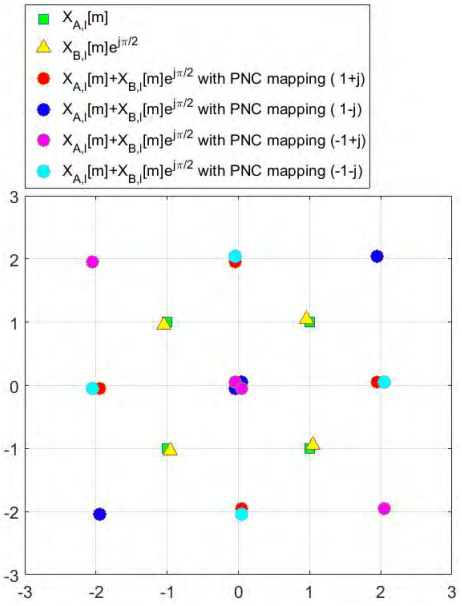

FIGURE 2. Constellation sample of PNC system (QPSK).

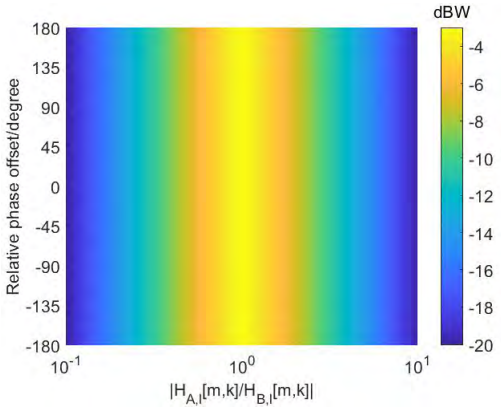

FIGURE 3. The power level under different relative channel gain (BPSK).

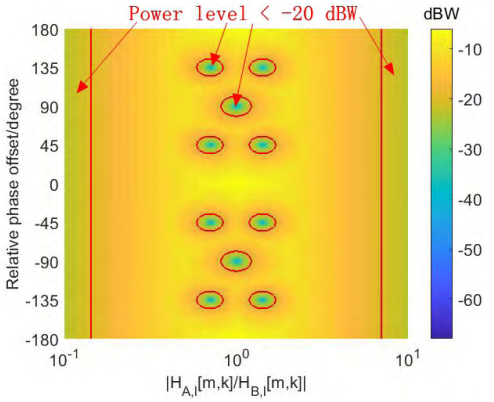

FIGURE 4. The power level under different relative channel gain (QPSK).

channel estimation [22] considers ICI as part of the noise, but here we attempt to achieve an ICI-aware scheme for channel estimation, detection and decoding to mitigate the negative effect of CFO.

C. RELATIVE CHANNEL GAIN IN PNC RECEIVER

This subsection studies the impact of relative channel gain in XOR mapping. Fig. 2 plots the received constellation of the superimposed QPSK signals without neither noise nor ICI.

In this sample, the relative channel is $\frac{\boldsymbol{H}_{A,I}[m,k]}{\boldsymbol{H}_{B,I}[m,k]} = e^{j\frac{\pi}{2}}$. To highlight different XOR mappings, we purposely set the phase offset slightly larger than $\frac{\pi}{2}$. The four points that belong to XOR mapping $(1+j)$ overlap with the four points that belong to $(-1-j)$. In this case, the minimum distance d_{min} of two different XOR mapping is equal to zero even in the absence of both noise and ICI. Compared with either SNR or SINR, the power level related to the minimum distance (referred to as 'the power level' in the following), which is defined as $10log10(\frac{1}{4}d_{min}^2)$, can better illustrate the performance of PNC systems.

Fig. 3 and 4 show the power level under diverse relative channel gains. The sum power of the two users is fixed at 0 dBW. For BPSK modulation, the power level is only determined by the power difference regardless of the phase offset. It decreases as the power difference increases. In the region with large power difference, the power level depends on the weak user whose power is relatively low. The power level is maximized when the amplitude ratio is equal to one. For QPSK modulation, the weak user determines the power level in the region with large power difference as well. But phase offset causes serious power level degradation in the power-balanced region, where the amplitude ratio is between 0.5 and 2. In the near power-balanced region, either 4 degree phase offset from 84 degree to 88 degree or 0.12 amplitude ratio offset from 0.81 to 0.93 can lead to 10 dB power level degradation. The area where the power level is lower than -20 dBW is highlighted in Fig. 4. Therefore, XOR mapping is sensitive to the relative channel gain, which includes both the power difference and phase offset.

D. ICI IN PNC RECEIVER

The power of ICI is determined by the maximum Doppler frequency and the shape of Doppler spectrum. For simplification, the two end nodes are assumed to share the same Doppler frequency and apply the Jakes' power spectrum. In addition, we only consider the ICI from two adjacent subcarriers since they dominate the ICI according to our study in [21]. According to [26, eq. (3.5)], the power of ICI given normalized received power can be written as

$$P_{ICI} = \int_{-f_d}^{f_d} \underbrace{\frac{1}{\pi f_d \sqrt{1-(f/f_d)^2}}}_{\text{Jake's Doppler power spectral density}} \times \underbrace{[sinc^2(1-f) + sinc^2(-1-f)]}_{\text{ICI from adjacent subcarriers}} df. \quad (8)$$

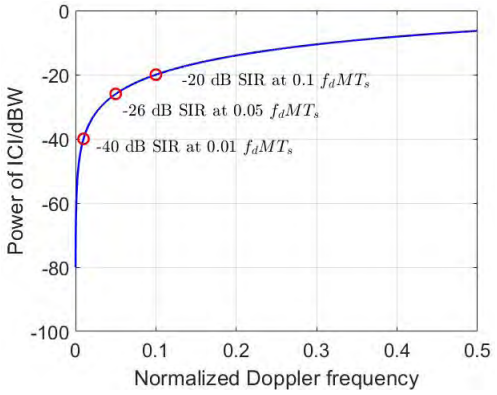

FIGURE 5. The power of ICI.

The first component on the right hand side (RHS) denotes the Jake's power spectral density function. The second component represents the interference from two adjacent subcarriers. The result of (8) is plotted in Fig. 5. Similar to Fig. 3 and 4, the sum power is fixed at 0 dBW.

For low normalized Doppler frequency $f_dMT_s < 0.05$ in VANETs, the power of ICI is lower than -26 dBW, the corresponding SIR is 26 dB. The power of ICI reaches -20 dBW when the normalized Doppler frequency is 0.1, and the corresponding SIR is 20 dB. Such SIR is high in conventional P2P communication systems. However, according to our study of relative channel gain in Fig. 4, -20 dBW ICI could be fatal to PNC systems. In the highlighted area in Fig. 4, ICI with $f_dMT_s = 0.1$ could already lead to error in XOR mapping.

Therefore, a robust PNC receiver in VANETs needs to accurately track the rapidly changing channel and provides ICI-aware estimation and decoding. To meet the requirement, BEM is applied in this paper to facilitate the task.

E. BASIS EXPANSION MODEL

Time-frequency-selective channels are inevitable in vehicular environments and challenging to estimate. It appears that the 802.11p pilot setup is infeasible to track the channel in rapid motion [7]. For PNC systems, each user is assigned with less pilot tones, which worsen the channel estimation. A strategy to address the issue of insufficient number of pilots is to exploit the data tone to improve the estimation [14]. The study in the previous two subsections reveals that the data decoding is more challenging in PNC systems regardless of noise, the data with error may deteriorate the channel estimation. This problem has never been studied in previous papers on BEM. In this work, we exploit the BEM to approximate the channels and it can transform (6) into a linear equation, which is much easier to solve. Specifically, the polynomial BEM (P-BEM) is assumed. We can re-write the complex channel gain $c_{p_i}(t)$ of G_z OFDM symbols by applying P-BEM as

$$c_{p_i}(qT_s) = \sum_{g=1}^{G_z} \theta_{p_i,g} q^{g-1} + \xi[q] \tag{9}$$

where $\theta_{p_i,g}$ is a polynomial coefficient to establish the target channels, and $\xi[q]$ is the approximation error. Compared with estimating $c_{p_i}(qT_s)$ under all possible q, we can easily compute it once the polynomial coefficients are known. And thus, the output coefficient $\alpha_t(k, z, m, p_i)$ can be estimated according to (6). Here, we can completely reconstruct the impulse response matrix $\boldsymbol{H}$ if the delay spread τ_{p_i} is also known. Thus, the channel estimation is equivalent to calculating the delay spread τ_{p_i} and the polynomial coefficient $\theta_{p_i,g}$. The impulse response in (6) can be re-written after applying P-BEM as

$$\begin{aligned}\boldsymbol{H}_{i,l}[m,k] = &\sum_{p_i=1}^{P_i}\sum_{g=1}^{G_z}\{e^{-j2\pi k\Delta f\tau_{p_i}} \\ &\times \sum_{q=0}^{M-1}(q-M+l(M+G))^{g-1}e^{j2\pi\frac{k-m}{M}q}\}\theta_{p_i,g}.\end{aligned} \tag{10}$$

And we can further transform it to the linear form

$$\boldsymbol{H}_{i,l}[m,k] = \boldsymbol{\alpha}(m,k,l,i)\boldsymbol{\theta}_i, \tag{11}$$

whith

$$\begin{aligned}\boldsymbol{\alpha}(m,k,l,i) &= [\alpha_{p_1,1}(m,k), \alpha_{p_1,2}(m,k), \ldots, \alpha_{p_1,G_z}(m,k) \\ &\quad \alpha_{p_2,1}(m,k), \ldots, \alpha_{P_i,G_z}(m,k)], \\ \alpha_{p_i,g}(m,k) &= e^{-j2\pi k\Delta f\tau_{p_i}} \\ &\quad \sum_{q=0}^{M-1}(q-M+l(M+G))^{g-1}e^{j2\pi\frac{k-m}{M}q}, \\ \boldsymbol{\theta}_i &= [\theta_{p_1,1}, \theta_{p_1,2}, \ldots, \theta_{p_1,G_z}, \theta_{p_2,1}, \ldots, \theta_{P_i,G_z}]^T.\end{aligned} \tag{12}$$

Here $[.]^T$ indicates transpose, and in the remainder of this paper we use $[.]^H$ and $[.]^{-1}$ to denote hermitian transpose and inverse, respectively. Thus, we have demonstrated that the channel estimation problem for PNC in time-frequency selective channels can be considered as resolving a linear problem. And once the delay spread is known, both $\boldsymbol{\theta}^T = [\boldsymbol{\theta}_A, \boldsymbol{\theta}_B]$ and $\boldsymbol{H}$ can denote the channel information, and thus they can be treated equivalently.

IV. THE PROPOSED ICI-AWARE SCHEME

This paper proposes an iterative method to jointly address two issues. The first one is to accurately estimate the complicated mobile radio channels with pilot and data tones. The second one is to detect and decode the transmitted data $\boldsymbol{S} = [\boldsymbol{S}_A, \boldsymbol{S}_B]^T$ given channel information $\boldsymbol{H}$ and received data $\boldsymbol{Y}$. $\boldsymbol{S}$ is a three dimensional array containing element $\boldsymbol{S}_{i,l}[m]$. Similarly, $\boldsymbol{Y}$ is a two dimensional matrix including element $\boldsymbol{Y}_l[m]$ and $\boldsymbol{H}$ is a four dimensional array containing element $\boldsymbol{H}_{i,l}[m,k]$. Accordingly, we divide the system into two phases:

Channel estimation phase: Through exploiting the information in pilot and data tones, this phase aims to obtain the optimal channel information with the maximum a posteriori (MAP) probability $\hat{\boldsymbol{H}}_{MAP} = \arg\max_{\boldsymbol{H}} p(\boldsymbol{H}|\boldsymbol{Y}) =$

$\arg\max_{\boldsymbol{H}} \sum_{\boldsymbol{S}} p(\boldsymbol{H}, \boldsymbol{S}|\boldsymbol{Y})$. This optimization problem is resolved by applying the EM algorithm and P-BEM.

Detection and decoding phase: With the MAP channel information $\hat{\boldsymbol{H}}_{MAP}$ calculated in the channel estimation phase, the goal of this phase is to find the MAP probability $p(\boldsymbol{S}|\hat{\boldsymbol{H}}_{MAP}, \boldsymbol{Y})$. The BP algorithm is used in this phase to mitigate the effect of ICI.

As can be seen, the detection and decoding phase requires the MAP $\hat{\boldsymbol{H}}_{MAP}$ calculated in the channel estimation phase. In turn, the calculation of $\hat{\boldsymbol{H}}_{MAP}$ requires the APP of $\boldsymbol{S}$, which is generated in the detection and decoding phase. The proposed scheme iterates between the two phases.

A. CHANNEL ESTIMATION PHASE

This paper aims to estimate time-frequency-selective channels. For time-varying channels, many previous works on channel estimation [16], [27] characterized the delay spread as discrete-time channel taps, and the taps can be calculated with preambles and pilots. In this paper, we employ the same model, both preambles and pilots are separated from the two end nodes. Thus, we can apply the conventional methods [16] to calculate the delay taps. The complexity of the delay measurement algorithm is low, and thus feasible for time-critical applications. Notice that the availability of delay information is commonly assumed in papers on BEM-based channel estimation [17], [27] to focus on the analysis of BEM. Similarly, in this work, we focus on studying the proposed algorithm and assume that the number of paths and the corresponding delays are known in the simulation. For the experiment, the delay measurement algorithm [16] is implemented and the output is fed to the proposed scheme.

OFDM modulated systems divide frequency spectrum into multiple subcarriers to carry information. Subcarriers inserted with known data are pilot tones and others are either data tones or null tones (e.g., the DC subcarrier is normally unused). The channel information $\boldsymbol{H}$ can be estimated more accurately by inserting more pilots, but this reduce the available bandwidth for data transmission. Owing to the time-frequency-selective channels and CFOs, it is difficult to track the channel information with pilots only. Our solution is to take advantage of data tones to optimize the channel estimation. It can also further mitigate the negative effect of ICI.

In the EM algorithm, the transmitted data $\boldsymbol{X}$ is the latent (or hidden variable), the received signal $\boldsymbol{Y}$ is the observed data, and the channel information $\boldsymbol{H}$ is the hidden parameter. The auxiliary function in the EM algorithm is used to calculate the expected value of the log-likelihood of the desired data given the current estimated channel. There are three stages as follows:

1. Initialization stage: find the initial channel information $\boldsymbol{H}^{init}$.

2. Expectation stage (E-stage): given the previous estimation $\boldsymbol{H}^{old}$, evaluate the auxiliary function

$$Q(\boldsymbol{H}|\boldsymbol{H}^{old}) = \sum_{\boldsymbol{S}} p(\boldsymbol{S}|\boldsymbol{Y}, \boldsymbol{H}^{old}) \log p(\boldsymbol{S}, \boldsymbol{Y}|\boldsymbol{H}). \quad (13)$$

3. Maximization stage (M-stage): optimize the channel parameters $\boldsymbol{H}^{new}$ by maximizing the auxiliary function

$$\boldsymbol{H}^{new} = \arg\max_{\boldsymbol{H}} Q(\boldsymbol{H}|\boldsymbol{H}^{old}). \quad (14)$$

For the initialization, only pilots are utilized to evaluate the channels. The procedure is similar to that of the M-stage by removing the data tones. Thus, we move to E-stage and offer more details to the calculation of the auxiliary function:

$$\begin{aligned} Q(\boldsymbol{H}|\boldsymbol{H}^{old}) &= \sum_{\boldsymbol{S}} p(\boldsymbol{S}|\boldsymbol{Y}, \boldsymbol{H}^{old}) \log p(\boldsymbol{S}, \boldsymbol{Y}|\boldsymbol{H}) \\ &= \sum_{\boldsymbol{X}} p(\boldsymbol{X}|\boldsymbol{Y}, \boldsymbol{H}^{old}) \log p(\boldsymbol{X}, \boldsymbol{Y}|\boldsymbol{H}) \\ &= \sum_{\boldsymbol{X}} p(\boldsymbol{X}|\boldsymbol{Y}, \boldsymbol{H}^{old}) \log p(\boldsymbol{Y}|\boldsymbol{X}, \boldsymbol{H}) \\ &\quad + \sum_{\boldsymbol{X}} p(\boldsymbol{X}|\boldsymbol{Y}, \boldsymbol{H}^{old}) \log p(\boldsymbol{X}). \end{aligned} \quad (15)$$

The source data $\boldsymbol{S}$ is replaced with encoded data $\boldsymbol{X}$ because we care about the specific information contained in each subcarrier. The component $\sum_{\boldsymbol{X}} p(\boldsymbol{X}|\boldsymbol{Y}, \boldsymbol{H}^{old}) \log p(\boldsymbol{X})$ is irrelevant to the channel matrix $\boldsymbol{H}$. It thus can be neglected and removed in the M-stage. The auxiliary function can be re-written as follows:

$$Q(\boldsymbol{H}|\boldsymbol{H}^{old}) \propto \sum_{\boldsymbol{X}} p(\boldsymbol{X}|\boldsymbol{Y}, \boldsymbol{H}^{old}) \log p(\boldsymbol{Y}|\boldsymbol{X}, \boldsymbol{H}) \quad (16)$$

where the component $p(\boldsymbol{X}|\boldsymbol{Y}, \boldsymbol{H}^{old})$ is the posteriori probability which can be calculated during the detection and decoding phase. To better analyze the auxiliary function, we re-write it as the summation of sub-auxiliary functions of individual symbols.

$$Q(\boldsymbol{H}|\boldsymbol{H}^{old}) = \sum_{l=1}^{L} Q(\boldsymbol{H}_l|\boldsymbol{H}_l^{old}). \quad (17)$$

The global auxiliary function is equivalent to multiple sub-auxiliary functions, and the sub-auxiliary functions for individual symbols can be evaluated based on their corresponding posteriori probability $p(\boldsymbol{X}_l|\boldsymbol{Y}, \boldsymbol{H}^{old})$.

We prove in Section III that the channel information $\boldsymbol{H}$ is equivalent to the P-BEM coefficients $\boldsymbol{\theta}$ when the delay spread is known, and we further assume that the delay taps are obtained in advance in this work. Thus, the maximization of $Q(\boldsymbol{H}|\boldsymbol{H}^{old})$ is equal to the optimization of $Q(\boldsymbol{\theta}|\boldsymbol{\theta}^{old})$. In the following mathematical derivation, the optimization problem is considered in a group consisting multiple sub-auxiliary functions. This means channel estimation runs in each group, which including G_z successive symbols. For one group, the Q function, namely the auxiliary function, is equal to the sum of G_z sub-auxiliary function

$$Q(\boldsymbol{H}|\boldsymbol{H}^{old}) \propto \sum_{g=1}^{G_z} \sum_{\boldsymbol{X}_g} \sum_{m=-M/2}^{M/2-1} p(\boldsymbol{X}_g|\boldsymbol{Y}, \boldsymbol{H}^{old})$$

$$\times\{-|\boldsymbol{Y}_g[m]-\sum_i\sum_{k=-M/2}^{M/2-1}\boldsymbol{H}_{i,g}[m,k]\boldsymbol{X}_{i,g}[k]|^2/(2\sigma_f^2)\}. \tag{18}$$

Employing the P-BEM shown in (11), $\boldsymbol{H}_{i,g}[m,k]$ in (18) can be replaced with the P-BEM coefficient as follows.

$$\begin{aligned}&Q(\boldsymbol{H}|\boldsymbol{H}^{old})\\&\propto\sum_{g=1}^{G_z}\sum_{\boldsymbol{X}_g}\sum_{m=-M/2}^{M/2-1}p(\boldsymbol{X}_g|\boldsymbol{Y},H^{old})\{-|\boldsymbol{Y}_g[m]\\&\quad-\{\sum_{k=-M/2}^{M/2-1}[\boldsymbol{\alpha}(m,k,g,A)\boldsymbol{X}_{A,g}[k],\boldsymbol{\alpha}(m,k,g,B)\boldsymbol{X}_{B,g}[k]]\}\\&\quad\times[\boldsymbol{\theta}_A,\boldsymbol{\theta}_B]^T|^2/(2\sigma_f^2)\}.\end{aligned} \tag{19}$$

To optimize the above Q function, we make the associated derivative to be zero as shown in (20), as shown at the bottom of the next page. $\hat{\boldsymbol{X}}_{i,g}[k]$ is the posteriori expectation of the transmitted data after decoding. Let $\boldsymbol{Y}_G$ contains the received frequency-domain data of a group. Since each group includes G_z symbols and each symbol contains M tones, $\boldsymbol{Y}_G$ is a $(MG_z)\times 1$ vector. $\boldsymbol{A}_G$ is a $\{MG_z\}\times\{(P_A+P_B)G_z\}$ matrix with row vector $\sum_{k=-M/2}^{M/2-1}[\boldsymbol{\alpha}(m,k,g,A)\hat{\boldsymbol{X}}_{A,g}[k],\boldsymbol{\alpha}(m,k,g,B)\hat{\boldsymbol{X}}_{B,g}[k]]$. Referring to (20), each element in $\boldsymbol{Y}_G$ has the corresponding row vector in $\boldsymbol{A}_G$. (20) can be simplified as

$$\boldsymbol{Y}_G=\boldsymbol{A}_G\boldsymbol{\theta}+\boldsymbol{\Xi} \tag{21}$$

where $\boldsymbol{\Xi}$ is the estimation error vector due to noise and approximation error in (9). We can maximize the auxiliary function by finding the optimal $\boldsymbol{\theta}$ to minimize the error $\boldsymbol{\Xi}$. To this end, we use a minimum mean square error (MMSE) estimator to achieve the optimization. According to [28, eq. (26)], the optimal $\boldsymbol{\theta}$ is calculated as

$$\boldsymbol{\theta}^{new}=(\boldsymbol{A}_G+\boldsymbol{\Sigma}_n(\boldsymbol{A}_G^H)^{-1}\boldsymbol{\Sigma}_{\boldsymbol{\theta}}^{-1})^{-1}\boldsymbol{Y}_G \tag{22}$$

where $\boldsymbol{\Sigma}_n$ and $\boldsymbol{\Sigma}_\theta$ are two covariance matrices for noise and $\boldsymbol{\theta}$, respectively. Since we assume the noise on each subcarrier is independent, the diagonal elements in $\boldsymbol{\Sigma}_n$ are $2\sigma_f^2$ and other elements are zero. Similarly, all propagation paths are uncorrelated and thus $\boldsymbol{\Sigma}_{\boldsymbol{\theta}}$ is a diagonal matrix on which the k-th diagonal element is $E(|\boldsymbol{\theta}[k]|^2)$. In each iteration of the EM algorithm, the channel estimation result from the previous iteration is used to calculate $\boldsymbol{\Sigma}_{\boldsymbol{\theta}}$.

So far, we have demonstrated the E-stage and M-stage of the EM algorithm. In the initialization stage, we can easily remove the data tones in (20) and perform (22) to obtain the channel information with pilots only. Besides, the covariance matrix $\boldsymbol{\Sigma}_{\boldsymbol{\theta}}$ is considered as an identity matrix at the beginning.

ICI compensation and equalization are common in conventional OFDM systems, but they are separated from the estimation of channel gains. Unlike the two methods, the proposed channel estimation takes ICI into consideration and evaluate the optimal P-BEM coefficient $\boldsymbol{\theta}$ to construct the channel matrix. Thus, it is ICI-aware channel estimation.

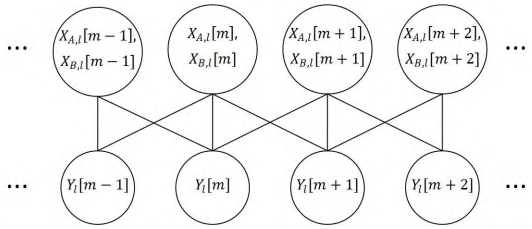

FIGURE 6. The Markov network for signal detection.

After performing channel estimation, the obtained channel information $\boldsymbol{H}$ will be used to conduct detection and decoding.

B. DETECTION AND DECODING PHASE

Given the estimated channel information $\boldsymbol{H}$, the proposed scheme conducts detection and decoding to acquire the transmitted data. Specifically, signals on each subcarriers are first detected and the APP of encoded data is obtained. Consequently, the APP is passed to the decoder to calculated the APP of source binary data. It means that both soft signal detection and channel decoding are performed in the proposed scheme. When CFO exists, the received signal on one subcarrier suffers ICI from other subcarriers. Traditional systems perform ICI compensation or equalization in advance, then signal detection is conducted on each subcarrier independently. This paper, by contrast, detects the signal by taking the ICI into account. To study the effect of ICI, we first construct a Markov network [29], [30] to represent the received signals on one symbol. Then, the sum-product BP algorithm is employed to conduct the inference to calculate the marginal probability of the transmitted data. After that, channel decoding is performed with the BP algorithm. The Markov network for signal detection is illustrated in Fig. 6.

As can be seen, factors $\boldsymbol{X}_{i,l}[m]$ on the upper row are hidden factors while factors $\boldsymbol{Y}_l[m]$ on the bottom row are observed factors. Each received signal $\boldsymbol{Y}_l[m]$ is connected to the corresponding subcarrier and two neighboring subcarriers. The reason why only three subcarriers are connected is that the received signal on one subcarrier mainly depends on the desired signal on the corresponding subcarrier and ICI from two adjacent subcarriers according to our studies in [21]. Connecting more subcarriers cannot significantly improve the performance but exponentially increases the computational complexity. The joint APP of encoded data from three successive subcarriers can be calculated and stored in $\boldsymbol{Y}_l[m]$ as follows:

$$\begin{aligned}&p(\boldsymbol{X}_l[m-1,m,m+1]|\boldsymbol{Y}_l[m],\boldsymbol{H}_l)\\&\propto\exp\{-|\boldsymbol{Y}_l[m]-\sum_i\sum_{u=m-1}^{m+1}\boldsymbol{H}_{i,l}[m,u]\boldsymbol{X}_{i,l}[u]|^2/2\sigma_f^2\}\end{aligned} \tag{23}$$

where $\boldsymbol{X}_l[m-1,m,m+1]$ denotes $\{\boldsymbol{X}_{A,l}[m-1,m,m+1],\boldsymbol{X}_{B,l}[m-1,m,m+1]\}$ and $\boldsymbol{H}_l$ is $\{\boldsymbol{H}_{A,l},\boldsymbol{H}_{B,l}\}$.

Thus, the factor $\boldsymbol{Y}_l[m]$ contains the APP $p(\boldsymbol{X}_l[m-1, m, m+1]|\boldsymbol{Y}_l[m], \boldsymbol{H}_l)$ of three successive subcarriers. The APP can be calibrated by performing sum-product message passing algorithm. After that, marginalization is conducted so that the marginal probability hidden in factor $\boldsymbol{X}_l[m]$ is obtained. It turns out that the BP algorithm detects the received signal by considering ICI from two neighboring subcarriers.

Here we provide more details with respect the the BP algorithm. For each observed factor $\boldsymbol{Y}_l[m]$ in Fig. 6, it contains the self-information $p(\boldsymbol{X}_l[m-1, m, m+1]|\boldsymbol{Y}_l[m], \boldsymbol{H}_l)$ and passes the self-information to two adjacent subcarriers. The passed self-information is called message, and the self-information is not passed directly. For instance, when factor $\boldsymbol{Y}_l[m]$ passes a message to $\boldsymbol{Y}_l[m+1]$, since $\boldsymbol{Y}_l[m+1]$ considers subcarriers m, $m+1$ and $m+2$, $\boldsymbol{Y}_l[m]$ only needs to pass the information related to these three subcarrers. Because $\boldsymbol{Y}_l[m]$ contains information regarding subcarriers $m-1, m$ and $m+1$, it needs to eliminate the information about subcarrier $m-1$ by performing marginalization. Let $\Psi_l[m]$ denotes the self-information in $\boldsymbol{Y}_l[m]$, the message generated by $\boldsymbol{Y}_l[m]$ and passed to $\boldsymbol{Y}_l[k]$ is indicated by $\zeta^l_{m\to k}$.

When the BP algorithm begins, messages are passed from the root down towards the leaves. In this work, the first message $\zeta^l_{1\to 2}$ is generated by $\boldsymbol{Y}_l[1]$ and passed to $\boldsymbol{Y}_l[2]$, then the shared variables in $\Psi_l[1]$ are kept while others are removed via variable elimination to obtain $\zeta^l_{1\to 2}$. After that, $\boldsymbol{Y}_l[2]$ updates itself to be the product of $\zeta^l_{1\to 2}$ and $\Psi_l[2]$. Then, $\boldsymbol{Y}_l[2]$ operates variable elimination and passes the new message $\zeta^l_{2\to 3}$ to the next factors $\boldsymbol{Y}_l[3]$. By continuously performing the same operation, the message is passed from the first factor to the last one. Consequently, the message is passed from the last factor back to the first one. When the bidirectional message passing is done, each factor updates itself as follows.

$$\beta_m = \Psi_l[m] \times \prod_{k\in Neighbor_m} \zeta^l_{k\to m} \tag{24}$$

where β_m is the updated belief, which can be considered as the calibrated APP. After marginalizing the belief, the marginal probability of hidden factor $\boldsymbol{X}_l[m]$ is obtained as the signal detection output. The structure of the factor graph considers ICI by connecting neighboring subcarriers, then the BP algorithm can calibrate the APP by mitigating the effect of noise and ICI. The results is passed to the channel decoder to decode the source data, and the APP of encoded data can be further calibrated via channel decoding.

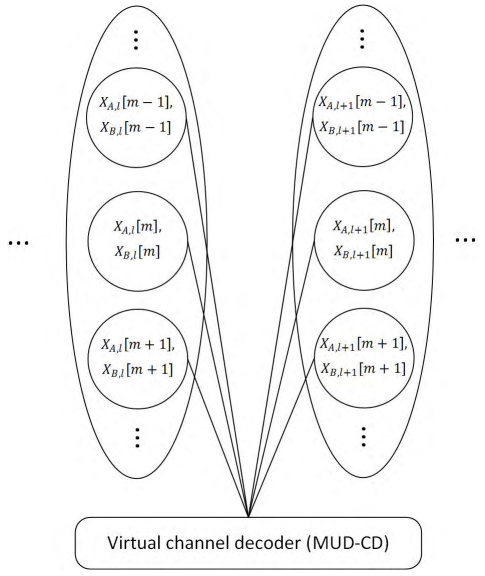

FIGURE 7. Virtual channel decoder based on MUD-CD.

With the APP of encoded data obtained, this work employs a virtual decoder [31] to perform the channel-decoding-network-coding (CNC) process. For the relay R in PNC, it needs to decoded the XOR output $X_R = X_A \oplus X_B$, and broadcasts X_R to the two end nodes in the downlink phase. Therefore, There are two ways to perform CNC: 1) the XOR APP is first calculated based on the output of signal detection, then the XOR output of the source data $S_R = S_A \oplus S_B$ is decoded and encoded for the downlink phase; 2) the channel decoding is performed based on the APP, which means that S_A and S_B are both decoded jointly. Then according to the decoding results, network coding and channel encoding are performed. With respect to [31], the two methods are called XOR-CD and MUD-CD respectively, and it was shown that MUD-CD outperforms XOR-CD. In this work, MUD-CD is preferred since it does not only provide better performance but also the APP of data from the two end nodes, which is required in the channel estimation phase. Fig. 7 shows that all encoded data in a frame are connected to the virtual channel decoder to perform CNC based on MUD-CD.

In CNC, after operating channel decoding, both the improved APP of encoded data (X_A, X_B) and that of source

$$\frac{dQ(\boldsymbol{H}|\boldsymbol{H}^{old})}{d\boldsymbol{\theta}} = 0$$
$$\sum_{g=1}^{G_z}\sum_{\boldsymbol{X}_g}\sum_{m=-M/2}^{M/2-1} p(\boldsymbol{X}_g|\boldsymbol{Y}, \boldsymbol{H}^{old})(\boldsymbol{Y}_g[m] - \{\sum_{k=-M/2}^{M/2-1}[\boldsymbol{\alpha}(m,k,g,A)\boldsymbol{X}_{A,g}[k], \boldsymbol{\alpha}(m,k,g,B)\boldsymbol{X}_{B,g}[k]]\}[\boldsymbol{\theta}_A, \boldsymbol{\theta}_B]^T) = 0$$
$$\sum_{g=1}^{G_z}\sum_{m=-M/2}^{M/2-1}(\boldsymbol{Y}_g[m] - \{\sum_{k=-M/2}^{M/2-1}[\boldsymbol{\alpha}(m,k,g,A)\hat{\boldsymbol{X}_{A,g}}[k], \boldsymbol{\alpha}(m,k,g,B)\hat{\boldsymbol{X}_{B,g}}[k]]\}\boldsymbol{\theta}) = 0. \tag{20}$$

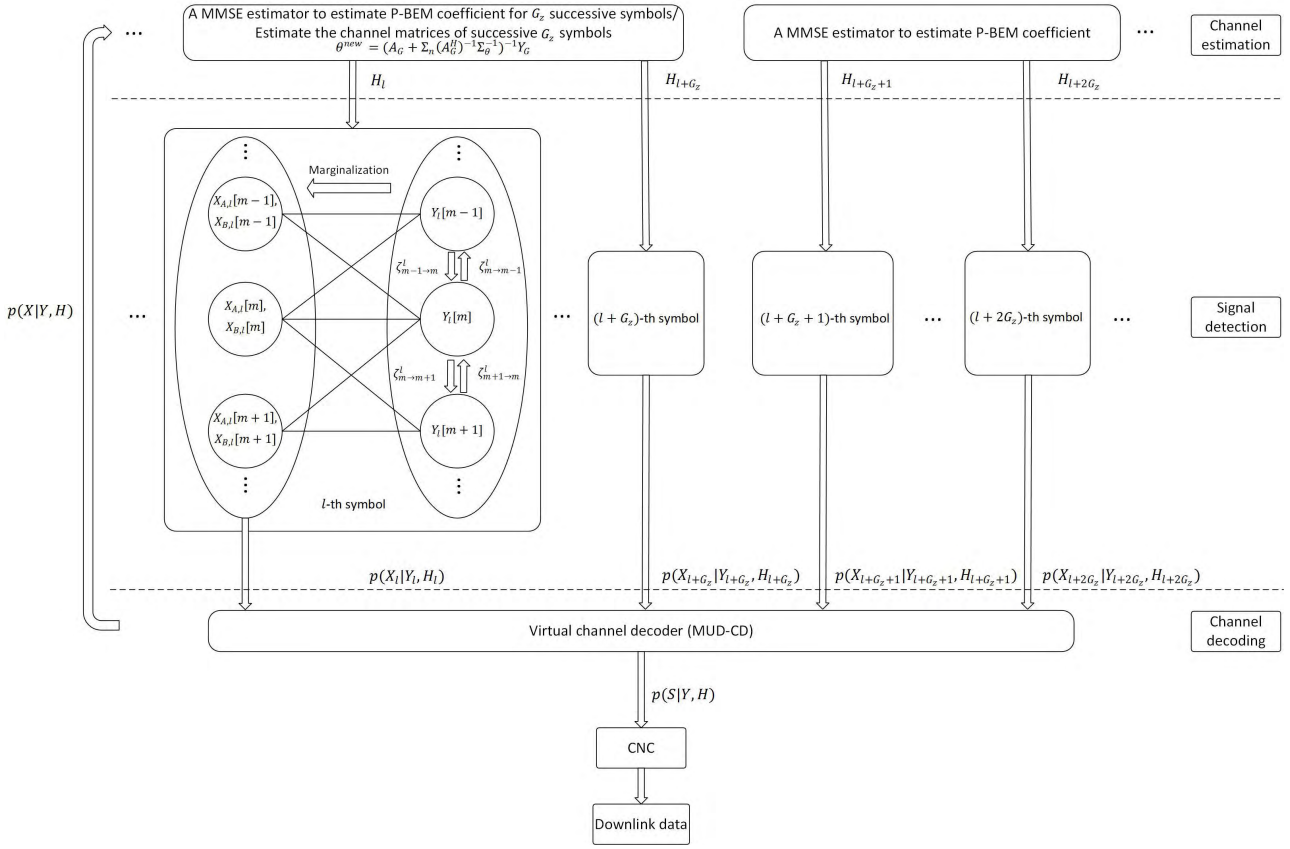

FIGURE 8. Factor graph of the proposed scheme.

data (S_A, S_B) are obtained. For the last iteration of the proposed scheme, the APP of source data (S_A, S_B) is used to run network coding and channel coding so that the downlink data is prepared for broadcasting. For other iterations, the APP of encoded data (X_A, X_B) is passed back for the channel estimation of the next iteration.

Since XOR is a linear operation, the virtual channel decoder can easily apply any linear channel codes such as LDPC code, lattice code and repeat accumulate (RA) code. In this paper, RA code is employed, and the RA decoder also applies the BP algorithm to decode the received data. However, any other linear channel codes are feasible in the proposed scheme. So far, the procedures of channel estimation, signal detection and channel decoding have been introduced individually. Fig. 8 illustrates the architecture of the whole system.

The proposed method first estimates the P-BEM coefficient by constructing matrices $\boldsymbol{A}_G$, $\boldsymbol{\Sigma}_n$, $\boldsymbol{\Sigma}_\theta$ and $\boldsymbol{Y}_G$. The four matrices are discussed in (20) and (22). Then the full channel matrix $\boldsymbol{H}$ can be established according to (11), and the output is used for signal detection. Given the channel information and received signals, the APP of the encoded data is calculated and stored in factor $\boldsymbol{Y}_l[m]$. After that, sum-product message passing is implemented in each symbol individually and we can observe the forward messages $\zeta^l_{m\to m+1}$ and the backward messages $\zeta^l_{m+1\to m}$. After performing inference, marginalization is operated to obtain the marginal probability $p(\boldsymbol{X}_l|\boldsymbol{Y}_l, \boldsymbol{H}_l)$. This ICI-aware signal detection technique mitigates the negative effect of CFO, and then the APP is delivered to the virtual channel decoder for CNC. Channel coding can significantly improve the reliability of the APPs $p(\boldsymbol{X}|\boldsymbol{Y}, \boldsymbol{H})$ and $p(\boldsymbol{S}|\boldsymbol{Y}, \boldsymbol{H})$. And thus we can apply the enhanced $p(\boldsymbol{X}|\boldsymbol{Y}, \boldsymbol{H})$ to perform a better channel estimation. The proposed system runs iteratively between the above phases and $p(\boldsymbol{S}|\boldsymbol{Y}, \boldsymbol{H})$ is expected to converge at the true value. Then by simply performing network coding and channel encoding, the XOR output is prepared to be broadcasted in the downlink phase.

V. COMPLEXITY ANALYSIS

Here we analyze the computational complexity of the proposed scheme. We divide the proposed scheme into three parts: 1) The channel estimation part; 2) The signal detection part and 3) The channel decoding part. The complexity is summarized in Table 1. In addition to the ICI-aware approach, a conventional scheme (Conv) is provided for reference. The details of the algorithm is discussed in the next section. The complexity of Conv is close to the PNC prototype in [8] and the IEEE 802.11p standard.

TABLE 1. Complexity of one frame.

Algorithm	ICI-aware	Conv
Channel estimation	$\mathcal{O}(MLG_z^2(M+P_A+P_B)(P_A+P_B)+2ML(M+M^2G_z^2+P_AG_z+P_BG_z))$	$\mathcal{O}(2ML)$
Signal detection	$\mathcal{O}(12\Omega_A^3\Omega_B^3ML)$	$\mathcal{O}(\Omega_A\Omega_BML)$
Channel decoding	$\mathcal{O}(ML\Omega_A\Omega_B(2\Omega_A\Omega_B-1))$	$\mathcal{O}(ML\Omega_A\Omega_B(2\Omega_A\Omega_B-1))$

For the channel estimation part, the channel information is calculated via equation (22). Component $\boldsymbol{A}_G$ needs $\mathcal{O}(2m^2G_z)$ multiplications, where $\alpha(m,k,g,i)$ can be pre-computed and stored. Similarly, component $\boldsymbol{\Sigma}_n$ can be pre-computed and component $\boldsymbol{\Sigma}_\theta^{-1}$ is obtained from the previous iteration. We can see that there are three multiplications, one addition and two inverse operations in (22). By assuming the Moore-Penrose pseudoinverse of an $m \times n$ matrix that requires $\mathcal{O}(max(m,n)^3)$ computations, the product of an $m \times n$ matrix and an $n \times k$ matrix needs $\mathcal{O}(mnk)$ computations and the addition of the two $m \times n$ matrices requires $\mathcal{O}(mn)$ computations, the complexity of (22) is $\mathcal{O}(MLG_z^2(M+P_A+P_B)(P_A+P_B)+2ML(M+M^2G_z^2+P_AG_z+P_BG_z))$. The Moore-Penrose pseudoinverse is the most computationally expensive operation in the channel estimation part, but we can reduce the complexity by utilizing faster pseudoinverse algorithm, and the complexity can be further reduced by replacing the MMSE estimator with LS estimator.

For the signal detection part, based on the constructed graphical model shown in Fig. 6, this part has three steps: APP calculation, message passing and marginalization. For one group containing G_z symbol, the APP calculation requires $\mathcal{O}(7ML\Omega_A^3\Omega_B^3)$ operations, where Ω_A and Ω_B are the alphabet size of modulation for two end nodes. For instance, $\Omega_i = 2$ when BPSK is applied and $\Omega_i = 4$ when QPSK is applied. Then, for sum-product message passing algorithm, we need to compute the sum and product of APP, this step needs $\mathcal{O}(4ML\Omega_A^3\Omega_B^3)$ computations. The last step is marginalization and it takes $\mathcal{O}(ML\Omega_A^3\Omega_B^3)$ sum operations. Thus, the computational complexity of the signal detection part is $\mathcal{O}(12\Omega_A^3\Omega_B^3ML)$. The major complexity of the proposed scheme comes from the signal detection part, since the factor graph connect three successive subcarriers as shown in Fig. 6. Connecting less subcarriers can significantly decrease the complexity. For instance, we can just connect one neighboring subcarrier depending on the direction of the Doppler shift or consider the data from one end node for two neighboring subcarriers [21]. By doing so, the order of Ω_A and Ω_B will be reduced from three to two.

Coming to the channel decoding part, the complexity of this part bases on the type of channel code and decoding algorithm we utilize. In this paper we apply RA code and the complexity of is $\mathcal{O}(ML\Omega_A\Omega_B(2\Omega_A\Omega_B-1))$.

We can see that the configuration affects the complexity. For example, a large M significantly increases the complexity of the channel estimation, high-order modulation (e.g., 16-QAM) will make the signal detection dominates the complexity. We can control or reduce the complexity by adjusting the parameters in Table 1. For instance, we can see that the complexity of channel estimation shows a linear relationship to the square of the group size G_z^2. We will show in the next section (Fig. 9 and 10) that when G_z is reduced, the degradations in MSE and BER performances are minor.

Compared with the Conv algorithm, the proposed scheme shows higher complexity in the channel estimation and signal detection parts. However, the proposed scheme can perform individual channel estimation and signal detection in G_z successive symbols, thus the processing time can be significantly reduced with parallel computing hardware. For the implemented algorithms in MATLAB, the processing time of the proposed scheme is around 20 times of the Conv algorithm. This gap can be further decreased with optimized hardware.

VI. SIMULATION RESULTS

In this section, simulation is conducted to evaluate the performance of the proposed scheme. The testbed is implemented with MATLAB and follows the 802.11p standard. Several input parameters are controlled, thus the proposed scheme is verified under different scenarios. Specifically, we consider the maximum Doppler frequency f_{d_i}, the SNR, the group size G_z and the number of iteration. Through controlling the four parameters, we observe the bit error rate (BER) of the decoded XOR data and the mean square error (MSE) of the estimated channel gain $c_{p_i}(t)$. We first show the MSE and BER results with different G_z and configure a reasonable G_z for the following simulation. Then, the convergence speed is studied by observing both the MSE and BER after different number of iterations. After that, the proposed scheme and two benchmarks are compared under different f_{d_i} with both BPSK and QPSK modulations. In the following subsection, the simulation configuration is introduced.

A. SIMULATION CONFIGURATION

In terms of the time-frequency-selective channels, two independent five-path Rayleigh fading channels are simulated for the two end nodes A and B. The empirical parameters of RTV-Urban Canyon and Canyon Oncoming cases in [24] are utilized to characterize the delay spread and the path power for the two end nodes. The tap powers of the first path for the two cases are recored as 0 dB for simplification. Thus, 100 ns delay and -3 dB tap power are additionally added to all paths for node B. For each path in both A and B, we assume that the fading spectral shapes are Jakes' power spectrum with the same normalized Doppler frequency f_dMT_s. Table 2

TABLE 2. Time-frequency-selective channel parameters.

Path no.	Power (A)	Delay (A)	Power (B)	Delay (B)
1	0 dB	0 ns	-3 dB	100 ns
2	-11.5 dB	100 ns	-13.0 dB	201 ns
3	-19.0 dB	200 ns	-20.8 dB	301 ns
4	-25.6 dB	300 ns	-24.1 dB	400 ns
5	-28.1 dB	500 ns	-29.3 dB	500 ns

summarizes the fixed channel parameters for the two end nodes. Besides the Doppler frequency, the hardware frequency offset is considered. According to our empirical measurement, we set $f_{\delta_A} = 600$ Hz and $f_{\delta_B} = -600$ Hz for the two end nodes. It indicates 0.00864 and -0.00864 normalized CFO in the simulation.

Following the 802.11p standard, the simulation adopts 10 MHz bandwidth and operates on the 5.9 GHz band. The proposed scheme only utilizes pilot tones to estimate the channel at the first iteration, the number of pilot tones should be not less than $P_A + P_B$ according to (22). However, the 802.11p standard, which assigns only four subcarriers as pilot tones, cannot meet the requirement. Thus, we modify the pilot and data pattern in this work. Specifically, each symbol contains 144 subcarriers, which includes 120 data tones and 24 pilot tones. The pilots are time-orthogonal for the two end nodes, 12 pilot tones are assigned to node A and the other half is assigned to node B. All pilots are uniformly inserted into the symbol. The length of CP is configured as nine, which can successfully prevent ISI in the simulation. Both BPSK and QPSK modulations are considered in the simulation. Note that the 802.11p standard uses convolutional code with coding rate 1/2, 2/3 and 3/4, which is feasible for PNC systems as it is a linear channel code. However, we employed the regular RA code with coding rate 1/3 [14] in this work since the decoder is optimized for PNC systems by jointly decoding multiple users.

Besides the proposed approach (ICI-aware), two benchmarks are simulated for comparison. One conventional benchmark (Conv) employs the linear interpolation [32] for channel estimation and regards ICI as noise in detection and decoding. Specifically, each symbol estimates the channel responses independently. Two successive pilot tones are utilized to evaluate the channel responses for the data tones between them. Another benchmark (ICI-com) applies the same P-BEM as the proposed algorithm to estimate the whole channel response matrix for desired signals and ICI coefficients. However, only pilot tones are used for channel estimation as in [27]. In addition, soft interference cancellation is performed at the beginning of each iteration, the channel estimation and decoding parts are thus conducted assuming the absence of interference. For the proposed scheme, the BP algorithm is performed once in each signal detection and twice in each channel decoding. Table 3 summarizes the control variables considered in the simulation.

TABLE 3. Control parameters.

G_z	2, 3, 4
Number of iteration	1,2,3,4,5
$f_d M T_s$	0.06,0.12
Modulation	BPSK,QPSK

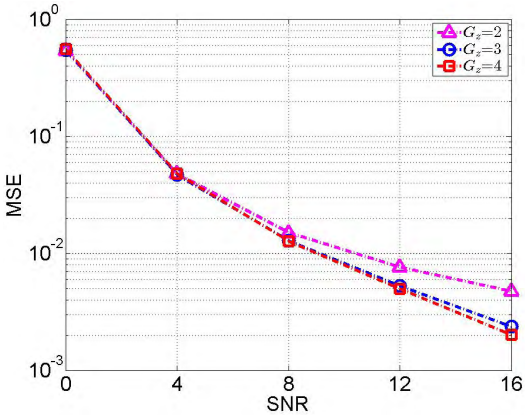

FIGURE 9. Comparison of MSE for different G_z.

B. GROUP SIZE STUDY

To select a reasonable G_z to balance the performance and computational complexity, we simulate the proposed ICI-aware approach with G_z from two to four. In this simulation, $f_d M T_s$ is set to be 0.12 and BPSK modulation is considered. The MSE and BER results after five iterations are shown in Fig. 9 and 10. We can see that the MSE decreases as the group size G_z increase. And the differences among the three curves widen when the SNR ascents. However, the gaps among them are small, especially in the low SNR regime. Compared with the MSE results, the BER results of the three G_z values are extremely close. The three BER curves almost overlap together in Fig. 10. It reveals that performance with different G_z are similar. Considering the computational complexity analyzed in the previous section, we set the G_z to be two in the following simulations.

C. CONVERGENCE SPEED AND INITIALIZATION STUDY

The proposed approach applies an iterative method for channel estimation, detection and decoding. The convergence speed is important since it determines the number of iterations required for convergence and affects the computational complexity. Applying the same configuration in the previous subsection, Fig. 11 and 12 shows the simulation results.

In Fig. 11, the MSE of the ICI-aware method becomes quiet stable after three iterations. It can be seen that the proposed scheme converges quickly in the low (e.g., 0 dB SNR) and high SNR (e.g., 12 dB) regimes, even one iteration is sufficient to converge. The medium SNR regime requires more iterations to converge. The reason is that in the low SNR regime, the proposed scheme cannot estimate the channel since the noise is too strong. In the high SNR regime,

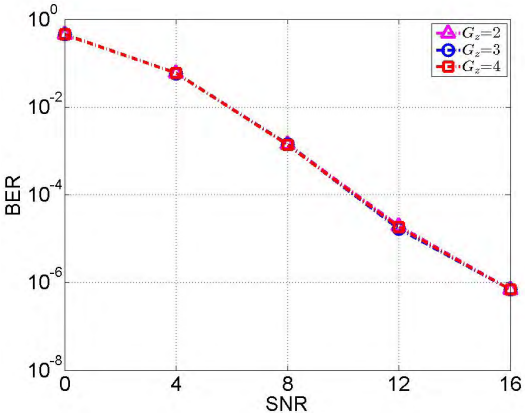

FIGURE 10. Comparison of BER for different G_z.

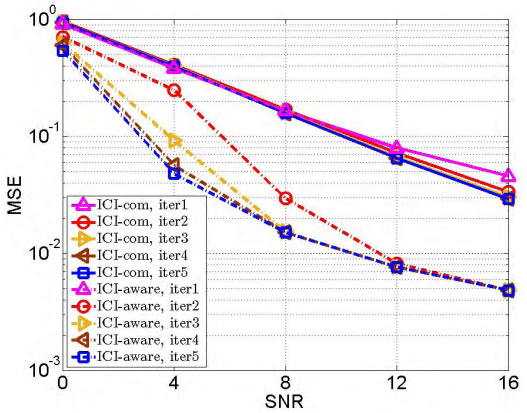

FIGURE 11. Comparison of MSE after different number of iterations.

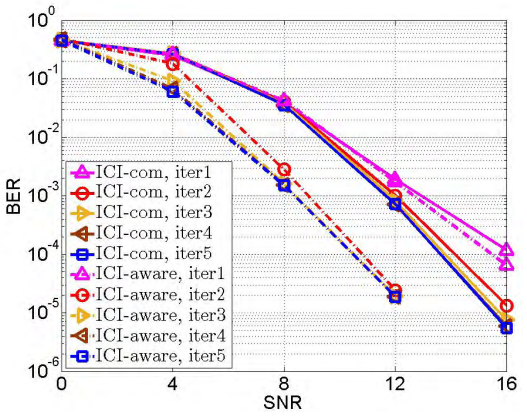

FIGURE 12. Comparison of BER after different number of iterations.

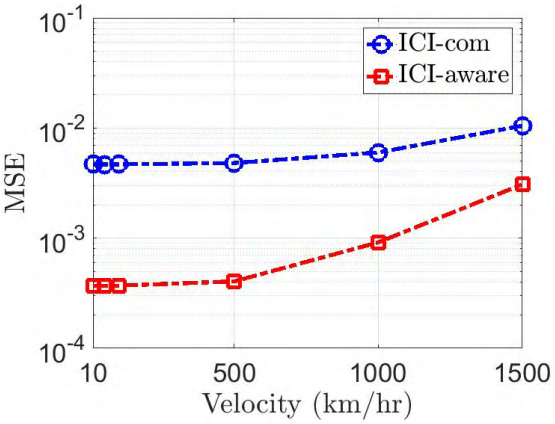

FIGURE 13. Comparison of MSE under different velocity.

the proposed scheme can efficiently evaluate the channel due to the weak noise. For the proposed scheme, it can converge within three iterations even in the worst case for the SNR between 0 and 12 dB. Similar trend is observed in the BER results shown in Fig. 12. We thus confirm that the proposed scheme can converge shortly, three iterations is already enough for the medium SNR regime and one iteration is acceptable in the low and high SNR regimes. The results of the ICI-com method are illustrated for comparison. We can see that the ICI-com method shows much worse performance and the results after different number of iterations are quiet close in the low and high SNR regimes. The reason is that the ICI-com method cannot efficiently evaluate the channel until the SNR reaches 12 dB. When the SNR reaches 16 dB, the ICI-com method can also converge after three iterations. Therefore, five iterations are sufficient to convergence for both the ICI-aware and ICI-com methods. We only show the results after five iterations in the remainder of this paper.

D. IMPACT OF VELOCITY ON BER AND MSE

After studying the group size and convergence speed, this subsection aims to study the impact of vehicular velocity on BER and MSE. To highlight the effect of velocity, we consider high SNR at 24 dB and perfect local oscillators to mitigate the effect of noise and CFOs from oscillators. The results are demonstrated in Fig. 13 and 14.

The velocity varies from 10 to 1500 km/hr. According to (2), the corresponding normalized Doppler frequency is from 0.0008 to 0.118. The velocity has a grater influence on the Conv algorithm than the other two algorithms. In the considered velocity range, the BER of Conv increases around 10 dB while the BER of the two BEM-based algorithms increases less than 4 dB. For velocity lower than 500 km/hr ($f_d MT_s \leq 0.0393$), the MSE and BER of the two BEM-based algorithms show slight perturbation. For velocity higher than 500 km/hr, the gap between the ICI-aware and ICI-com algorithm becomes smaller. Generally, the proposed scheme shows the best MSE and BER performance and is robust against velocity.

E. COMPARISON WITH BENCHMARKS

This subsection focuses on the comparison of the ICI-aware, ICI-com and Conv methods. The group size and the number of iterations are fixed to be two and five, respectively. Then simulations are conducted under different normalized

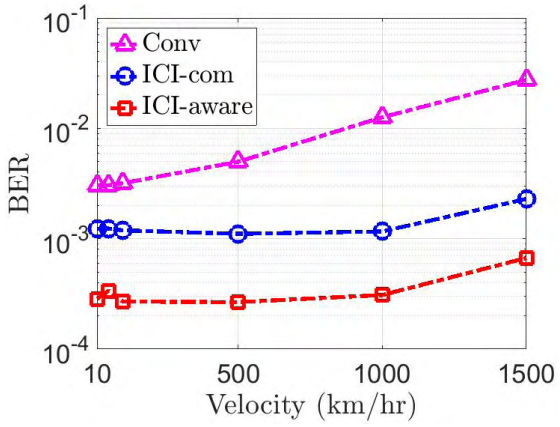

FIGURE 14. Comparison of BER under different velocity.

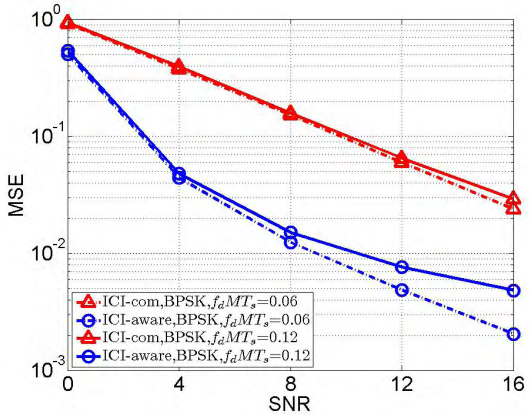

FIGURE 15. MSE results under different Doppler frequencies (BPSK modulation).

Doppler frequencies and modulations. BPSK modulation is first considered, the MSE and BER results are illustrated in Fig. 15 and 16. We can see that the normalized Doppler frequency is configured as 0.06 and 0.12. Following the 802.11p standard, relative velocity 200 km/hr would only cause 0.0157 normalized Doppler frequency. Therefore, $f_dMT = 0.06$ and 0.12 are quiet large numbers in vehicular networks, and more than sufficient to verify the performance of the proposed approach. For the MSE, the Conv method does not evaluate the time-domain channel gain $C_{p_i}(t)$, only the MSE results of the ICI-com and ICI-aware methods are shown. It can be seen that the MSE of the ICI-awre method is much smaller than that of the ICI-com method under different normalized Doppler frequencies. The MSE of the proposed scheme is even smaller than 0.01 when the SNR reaches 12 dB. Considering the BER results in Fig. 16, the proposed scheme outperforms the two benchmarks. Compared with the second best method, it provides around 4 dB SNR gain in the medium and high SNR regimes. An interesting point is that the BER curves of the ICI-aware method under different normalized Doppler frequency are almost the same. The reason is that the proposed approach can efficiently estimate the channels with the two Doppler frequencies, the MSE results in Fig. 15 also proves that the estimation is accurate, and the BER is mainly dominated by noise. In general, the proposed scheme offers best performance.

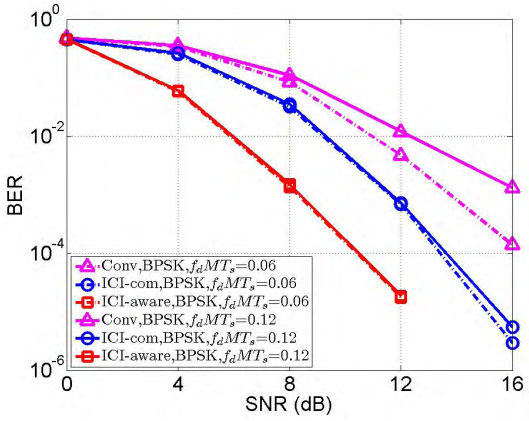

FIGURE 16. BER results under different Doppler frequencies (BPSK modulation).

Most OFDM systems employ high-order modulation such as QPSK and 16-QAM. We also evaluate the proposed scheme under QPSK modulation. The corresponding results are shown in Fig. 17 and 18.

Comparing the results of BPSK and QPSK modulations, the MSE and BER curves of the three methods show similar trend. The key different is that QPSK modulation suffers around 6 dB SNR penalty. In the low SNR regime (e.g., SNR is smaller than 8 dB), the MSE and BER results with QPSK modulation are considerable high. In the medium and high SNR regimes, the ICI-aware method outperforms the two benchmarks as with BPSK modulation.

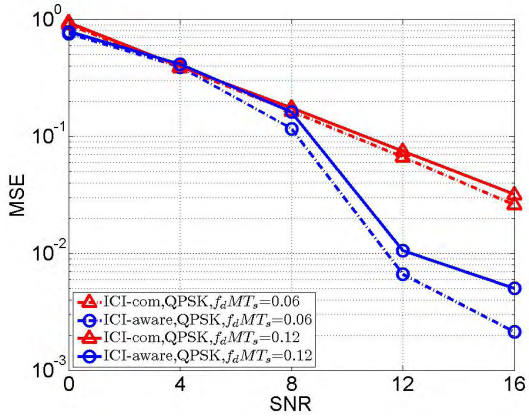

FIGURE 17. MSE results under different Doppler frequencies (QPSK modulation).

So far, the simulation results verify that the proposed scheme provides the best performance compared with the two benchmarks. The SNR gain comes from the consideration of ICI and the employment of data tones in channel estimation, signal detection and channel decoding. The fast convergence speed indicates that the computational complexity can be

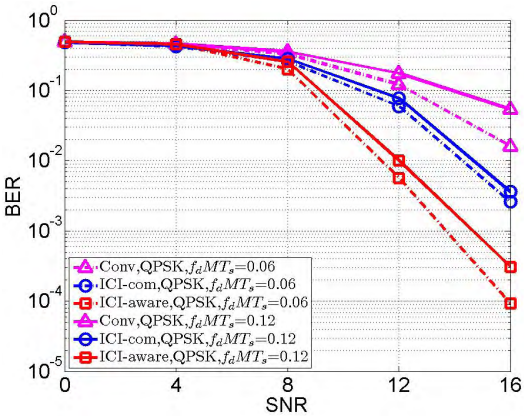

FIGURE 18. BER results under different Doppler frequencies (QPSK modulation).

FIGURE 19. The V2X experimental setup.

FIGURE 20. The V2P communication scenario.

FIGURE 21. The V2V communication scenario.

reduced by performing less iterations. For the high SNR regime, one iteration is acceptable for a five-path Rayleigh fading channel with 0.012 normalized Doppler frequency.

VII. EXPERIMENTAL RESULTS

To further evaluate the proposed scheme, we conduct an experiment along a road-side environment in the campus. The equipment for the experiment is shown in Fig. 19. We consider both the V2P and V2V communications through a road-side relay node and the snapshots of the two scenarios are shown in Fig. 20 and 21 respectively. For the V2V scenario, two cars A and B go toward the road junction at a speed of around 20 km/hr. Meanwhile, they transmit data to the relay R simultaneously.

In the experiment, we apply the PNC prototype in [8] to collect the overlapped signal. Specifically, the relay R broadcasts beacons periodically to the two end nodes. After receiving a beacon, the two end nodes transmit the predefined data, which apply the same modulation scheme and channel code as that of the simulation, to the relay R simultaneously. In the uplink phase, the two end nodes transmit data with the same transmission power, regardless of the radio channel and background noise. Thus, there is no perfect power control in the experiment, and the received power from the two end nodes can either be balanced or unbalanced. The relay R receives and saves the raw signals from the two end nodes. We then use the proposed scheme and the Conv algorithm, which are implemented on MATLAB, to process the raw data.

For the hardware, the PNC prototype runs on the universal soft radio peripheral (USRP) platform N210 and daughter board CBX-40. Each USRP is connected to a laptop T470p. The experiment is operated at the 5.9 GHz band and the bandwidth is 5 MHz.

The overlapping signals are processed off-line after the experiment. We implement the ESPRIT method [16] to detect the number of paths and the corresponding delays. To meet the time-critical V2X communications, we apply BPSK modulation to reduce the computational complexity. Other configurations are the same as that in the simulation section. We summarize the raw data collected from the two scenarios and process them with the Conv and ICI-aware algorithms. The normalized throughput is illustrated in Fig. 22.

The normalized throughput can be divided into four partitions: 1) ABX: this partition denotes that the individual information of the two end nodes (X_A and X_B) and the XOR output ($X_A \oplus X_B$) are successfully decoded; 2) X: this partition means that only the XOR output is decoded; 3) A|B: this partition indicates that only the individual information of either user (X_A or X_B) is decoded; 4) NONE: the last partition means that no packet is successfully decoded. For PNC systems, the combination of the ABX and X partitions represents the successful decoding rate.

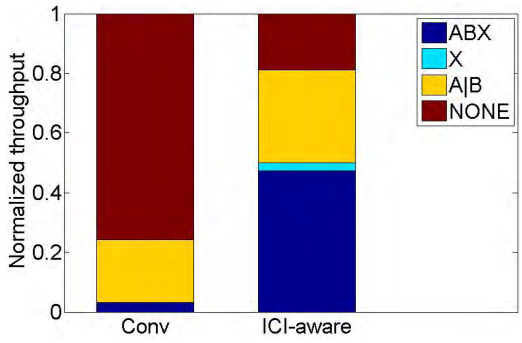

FIGURE 22. Normalized throughput of the experiment.

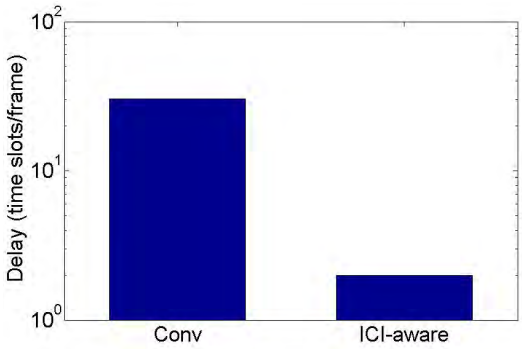

FIGURE 23. Communication delay of the experiment.

Fig. 22 shows that the ICI-aware algorithm provides around 0.5 normalized throughput for the PNC system. By contrast, the normalized throughput of the Conv method is relatively low, which is less than 0.04. An interesting point is that the partition of A|B is fairly large. For the ICI-aware algorithm, the A|B partition occupies around 20% of the received packets. One reason could be that we did not perform power control in the experiment, it is possible that the received power of one end node is too low that the corresponding data cannot be decoded while the received power of the other user is sufficient to be successfully decoded. For PNC systems, the partition of A|B indicates failure since PNC systems only require the XOR output of the two users. But conventional non-orthogonal multiple access (NOMA) [33] systems treat the individual information as important as well. This leads to our future work on the application of PNC in non-orthogonal V2X communications.

Latency is another significant criterion in time-critical V2X communications, thus the delay of the two algorithms are evaluated and shown in Fig. 23.

As can be seen, the delay of the ICI-aware algorithm is around 2 time slots/packet, while the theoretical minimum delay is 1 time slots/packet. By contrast, the delay of the Conv algorithm is up to 30 time slots/packet, which is too high for time-critical V2X applications.

VIII. CONCLUSION

This paper investigates the application of OFDM modulated PNC in V2X communications. The idea is to harness wireless interference to reduce latency and increase throughput in V2X communications. We aim to address two critical phenomena in this problem: the CFOs between multiple transmitters and receivers, and the time-frequency-selective channels in vehicular environment. Our solution is to exploit an ICI-aware approach that jointly achieves accurate channel estimation, signal detection, and channel decoding against the detrimental effects caused by the two phenomena. The channel estimation and detection and decoding phases are converted into two optimization problems. The first one is solved by the EM algorithm while the second one is tackled by the BP algorithm. The effect of ICI is considered in the two phases and the channel matrix is re-established for decoding, thus we claim that the proposed overall algorithm is ICI-aware.

Simulations and experiments are conducted to evaluated the proposed scheme. We first evaluate the tradeoff between performance and complexity of the proposed scheme and verify that the computational complexity can be reduced with minor performance degradation. Our results also indicate that the joint algorithm can converge within a small number of iterations (three to five). In the simulation that considers five-path double-selectively channels, the proposed scheme yields the lowest MSE and BER when compared with the benchmarks [27], [32]. In the real-world experiment, the joint algorithm continues to outperform the conventional algorithm. Our experimental results verify that the proposed algorithm is feasible for time-critical V2X communications and provide insights into our future work on non-orthogonal V2X communications.

REFERENCES

[1] Geographical Association. (2016). *The Case for Cellular V2X for Safety and Cooperative Driving*. [Online]. Available: http://5gaa.org/pdfs/5GAA-whitepaper-23-Nov-2016.pdf

[2] *3rd Generation Partnership Project Release 14*. Accessed: 2017. [Online]. Available: http://www.3gpp.org/release-14

[3] S. Zhang, S. C. Liew, and P. P. Lam, "Hot Topic: Physical-layer network coding," in *Proc. 12th Annu. Int. Conf. Mobile Comput. Netw.*, 2006, pp. 358–365.

[4] Z. Wang, J. Huang, S. Zhou, and Z. Wang, "Iterative receiver processing for OFDM modulated physical-layer network coding in underwater acoustic channels," *IEEE Trans. Commun.*, vol. 61, no. 2, pp. 541–553, Feb. 2013.

[5] H. Pan, L. Lu, and S. C. Liew, "Network-coded multiple access with high-order modulations," *IEEE Trans. Veh. Technol.*, vol. 66, no. 11, pp. 9776–9792, Nov. 2017.

[6] T. Koike-Akino, P. Popovski, and V. Tarokh, "Optimized constellations for two-way wireless relaying with physical network coding," *IEEE J. Sel. Areas Commun.*, vol. 27, no. 5, pp. 773–787, Jun. 2009.

[7] Z. Zhao, X. Cheng, M. Wen, B. Jiao, and C.-X. Wang, "Channel estimation schemes for IEEE 802.11p standard," *IEEE Intell. Transp. Syst. Mag.*, vol. 5, no. 4, pp. 38–49, Oct. 2013.

[8] L. Lu, T. Wang, S. C. Liew, and S. Zhang, "Implementation of physical-layer network coding," *Phys. Commun.*, vol. 6, pp. 74–87, Mar. 2013.

[9] Z. Tang, R. C. Cannizzaro, G. Leus, and P. Banelli, "Pilot-assisted time-varying channel estimation for OFDM systems," *IEEE Trans. Signal Process.*, vol. 55, no. 5, pp. 2226–2238, May 2007.

[10] J. S. Yedidia, W. T. Freeman, and Y. Weiss, "Understanding belief propagation and its generalizations," *Exploring Artif. Intell. New Millennium*, vol. 8, pp. 236–239, Jan. 2003.

[11] P. Popovski and H. Yomo, "The anti-packets can increase the achievable throughput of a wireless multi-hop network," in *Proc. IEEE Int. Conf. Commun.*, vol. 9, Jun. 2006, pp. 3885–3890.
[12] E. D. N. Ndih and S. Cherkaoui, "MAC for physical-layer network coding in VANETs," *Int. J. Bus. Data Commun. Netw.*, vol. 8, no. 4, pp. 84–106, 2012.
[13] I. W.-H. Ho, S. C. Liew, and L. Lu, "Feasibility study of physical-layer network coding in 802.11p VANETs," in *Proc. IEEE Int. Symp. Inf. Theory*, Jun. 2014, pp. 646–650.
[14] T. Wang and S. C. Liew, "Joint channel estimation and channel decoding in physical-layer network coding systems: An EM-BP factor graph framework," *IEEE Trans. Wireless Commun.*, vol. 13, no. 4, pp. 2229–2245, Apr. 2014.
[15] Y. Tan, S. C. Liew, and T. Huang, "Mobile lattice-coded physical-layer network coding with practical channel alignment," *IEEE Trans. Mobile Comput.*, vol. 17, no. 8, pp. 1908–1923, Aug. 2018.
[16] B. Yang, K. B. Letaief, R. S. Cheng, and Z. Cao, "Channel estimation for OFDM transmission in multipath fading channels based on parametric channel modeling," *IEEE Trans. Commun.*, vol. 49, no. 3, pp. 467–479, Mar. 2001.
[17] E. P. Simon, L. Ros, H. Hijazi, and M. Ghogho, "Joint carrier frequency offset and channel estimation for OFDM systems via the EM algorithm in the presence of very high mobility," *IEEE Trans. Signal Process.*, vol. 60, no. 2, pp. 754–765, Feb. 2012.
[18] L. Bernadó, T. Zemen, F. Tufvesson, A. F. Molisch, and C. F. Mecklenbräuker, "Delay and Doppler spreads of nonstationary vehicular channels for safety-relevant scenarios," *IEEE Trans. Veh. Technol.*, vol. 63, no. 1, pp. 82–93, Jan. 2014.
[19] M. Wu, F. Ludwig, M. Woltering, D. Wübben, A. Dekorsy, and S. Paul, "Analysis and implementation for physical-layer network coding with carrier frequency offset," in *Proc. 18th Int. ITG Workshop Smart Antennas*, Mar. 2014, pp. 1–8.
[20] M. Woltering, D. Wubben, and A. Dekorsy, "Physical layer network coding with Gaussian waveforms using soft interference cancellation," in *Proc. IEEE 81st Veh. Technol. Conf. (VTC Spring)*, May 2015, pp. 1–5.
[21] L. F. Xie, I. W.-H. Ho, S. C. Liew, L. Lu, and F. C. M. Lau, "The feasibility of mobile physical-layer network coding with BPSK modulation," *IEEE Trans. Veh. Technol.*, vol. 66, no. 5, pp. 3976–3990, May 2017.
[22] T. Wang, S. C. Liew, and L. You, "Joint phase tracking and channel decoding for OFDM PNC: Algorithm and experimental evaluation," in *Proc. ACM Workshop Softw. Radio Implement. Forum (SRIF)*, 2014, pp. 69–76.
[23] A. F. Molisch, F. Tufvesson, J. Kåredal, and C. F. Mecklenbräuker, "A survey on vehicle-to-vehicle propagation channels," *IEEE Commun. Mag.*, vol. 16, no. 6, pp. 12–22, Dec. 2009.
[24] G. Acosta-Marum and M. A. Ingram, "Six time- and frequency-selective empirical channel models for vehicular wireless LANs," *IEEE Veh. Technol. Mag.*, vol. 2, no. 4, pp. 4–11, Dec. 2007.
[25] M. Pätzold, *Mobile Fading Channels*, vol. 14. Hoboken, NJ, USA: Wiley, 2002.
[26] Y. Li and L. J. Cimini, "Bounds on the interchannel interference of OFDM in time-varying impairments," *IEEE Trans. Commun.*, vol. 49, no. 3, pp. 401–404, Mar. 2001.
[27] H. Hijazi and L. Ros, "Polynomial estimation of time-varying multipath gains with intercarrier interference mitigation in OFDM systems," *IEEE Trans. Veh. Technol.*, vol. 58, no. 1, pp. 140–151, Jan. 2009.
[28] B. Zhou and Q. Chen, "A tutorial on minimum mean square error estimation," Southwest Jiaotong Univ., Sichuan, China, Tech. Rep., 2015, doi: 10.13140/RG.2.1.4330.5444.
[29] F. R. Kschischang, B. J. Frey, and H.-A. Loeliger, "Factor graphs and the sum-product algorithm," *IEEE Trans. Inf. Theory*, vol. 47, no. 2, pp. 498–519, Feb. 2001.
[30] H.-A. Loeliger, J. Dauwels, J. Hu, S. Korl, L. Ping, and F. R. Kschischang, "The factor graph approach to model-based signal processing," *Proc. IEEE*, vol. 95, no. 6, pp. 1295–1322, Jun. 2007.
[31] S. C. Liew, S. Zhang, and L. Lu, "Physical-layer network coding: Tutorial, survey, and beyond," *Phys. Commun.*, vol. 6, pp. 4–42, Mar. 2013.
[32] S. Coleri, M. Ergen, A. Puri, and A. Bahai, "Channel estimation techniques based on pilot arrangement in OFDM systems," *IEEE Trans. Broadcast.*, vol. 48, no. 3, pp. 223–229, Sep. 2002.
[33] Y. Saito, Y. Kishiyama, A. Benjebbour, T. Nakamura, A. Li, and K. Higuchi, "Non-orthogonal multiple access (NOMA) for cellular future radio access," in *Proc. IEEE 77th Veh. Technol. Conf. (VTC Spring)*, Jun. 2013, pp. 1–5.

ZHENHUI SITU received the B.S. degree in electronic information science and technology from Sun Yat-sen University, Guangzhou, China, and the M.Sc. degree in electronic engineering from The Hong Kong University of Science and Technology, Hong Kong. He is currently pursuing the Ph.D. degree with the Department of Electronic and Information Engineering, The Hong Kong Polytechnic University. From 2014 to 2015, he was a Research Assistant with The Hong Kong Polytechnic University. His research interests include wireless communications and statistical signal processing, specifically in vehicular ad hoc networks (VANET). His most research focus is on the feasibility study of physical-layer network coding in VANETs.

IVAN WANG-HEI HO received the B.Eng. and M.Phil. degrees in information engineering from The Chinese University of Hong Kong, Hong Kong, in 2004 and 2006, respectively, and the Ph.D. degree in electrical and electronic engineering from the Imperial College London, London, U.K., in 2010. He was involved in the Mobile Environmental Sensing System Across a Grid Environment Project funded by the Engineering and Physical Sciences Research Council and the Department for Transport, U.K., and the International Technology Alliance Project funded by the U.S. Army Research Laboratory and the Ministry of Defence, U.K. He was a research intern with the IBM Thomas J. Watson Research Center, Hawthorne, NY, USA, in 2007, and a Postdoctoral Research Associate with the System Engineering Initiative, Imperial College London, in 2010. In 2010, he co-founded P2 Mobile Technologies Ltd., where he served as the Chief Research and Development Engineer. He is currently an Assistant Professor with the Department of Electronic and Information Engineering, The Hong Kong Polytechnic University, Hong Kong. His research interests include wireless communications and networking, specifically in vehicular ad-hoc networks, intelligent transportation systems, the Internet of Things, and physical-layer network coding. He primarily invented the MeshRanger series wireless mesh embedded system, which received the Silver Award in Best Ubiquitous Networking at the Hong Kong ICT Awards 2012. He is currently an Associate Editor of the IEEE Access and the IEEE Transactions on Circuits and Systems II, a TPC Co-Chair of the CoWPER Workshop in conjunction with IEEE SECON 2018, and a TPC Member of IEEE conferences (ICC, WCNC, and PIMRC).

TAOTAO WANG received the B.S. degree in electrical engineering from the University of Electronic Science and Technology of China, Chengdu, China, in 2008, the M.S. degree in information and signal processing from the Beijing University of Posts and Telecommunications, Beijing, China, in 2011, and the Ph.D. degree in information engineering from The Chinese University of Hong Kong, Hong Kong, in 2015. From 2015 to 2016, he was a Postdoctoral Research Fellow with the Institute of Network Coding, The Chinese University of Hong Kong. He joined the College of Information Engineering, Shenzhen University, as an Assistant Professor. His main research interests include wireless communications and networking, statistical signal, and data processing. He was a recipient of the Hong Kong Ph.D. Fellowship. He is a member of the IEEE.

SOUNG CHANG LIEW received the S.B., S.M., E.E., and Ph.D. degrees from the Massachusetts Institute of Technology. From 1984 to 1988, he was with the MIT Laboratory for Information and Decision Systems, where he investigated fiber-optic communications networks. From 1988 to 1993, he was with Telcordia, NJ, where he was engaged in broadband network research. Since 1993, he has been a Professor with the Department of Information Engineering, The Chinese University of Hong Kong. He is currently an Adjunct Professor with Peking University and with Southeast University, China. He is a Consultant with the Hong Kong Applied Science and Technology Research Institute, providing technical advice and helping to formulate research and development directions and strategies in the areas of wireless internetworking, applications, and services. Separately, TCP Veno, a version of TCP to improve its performance over wireless networks proposed by his research group, has been incorporated into a recent release of Linux OS. He initiated and built the first inter-university ATM network testbed in Hong Kong, in 1993. His research group pioneers the concept of physical-layer network coding. Besides academic activities, he is active in the industry. He co-founded two technology start-ups in Internet software and serves as a consultant for many companies and industrial organizations. He holds nine U.S. patents. His research interests include wireless networks, Internet protocols, multimedia communications, and packet switch design. He is a Fellow of the IEEE, the IET, and the HKIE. His research group received best paper awards from IEEE MASS 2004 and IEEE WLN 2004. He was a recipient of the first Vice-Chancellor Exemplary Teaching Award, in 2000, and the Research Excellence Award at The Chinese University of Hong Kong, in 2013. He currently serves as an Editor for the IEEE TRANSACTIONS ON WIRELESS COMMUNICATIONS and the *Ad Hoc and Sensor Wireless Networks*.

SID CHI-KIN CHAU received the B.Eng. degree from The Chinese University of Hong Kong and the Ph.D. degree from the University of Cambridge. He was an Associate Professor with the Department of Computer Science, Masdar Institute, Khalifa University of Science and Technology; a Visiting Professor with MIT; and a Senior Research Fellow with the Institute for Infocomm Research, A*STAR, Singapore. He was a Visiting Scholar with the IBM T. J. Watson Research Center, Hawthorne, USA, and with Raytheon-BBN Technologies, Boston, USA. He is currently a Senior Lecturer with The Australian National University. His research involved in the broad areas of optimization, algorithms, and the Internet-of-Things systems for applications of sustainability and energy systems, such as smart buildings, smart grid, and intelligent transportation. He is a TPC Member of top international conferences in smart energy systems and smart cities, such as the ACM eEnergy and ACM BuildSys. He was a TPC Chair of ACM eEnergy 2018.